



1 Annual changes in plant functional types and their responses to climate  
2 change on the Northern Tibetan Plateau

3

4 Lan Cuo<sup>1</sup>, Yongxin Zhang<sup>2</sup>, Shilong Piao<sup>3</sup> Yanhong Gao<sup>4</sup>

5 <sup>1</sup>Center for Excellence in Tibetan Plateau Earth Sciences, Key Laboratory of Tibetan  
6 Environment Changes and Land Surface Processes, Institute of Tibetan Plateau Research,  
7 Chinese Academy of Sciences, Beijing, China,

8 <sup>2</sup>Research Applications Laboratory, National Center for Atmospheric Research, Boulder,  
9 Colorado, USA

10 <sup>3</sup>Center for Excellence in Tibetan Plateau Earth Sciences, Key Laboratory of Tibetan  
11 Environment Changes and Land Surface Processes, Institute of Tibetan Plateau Research,  
12 Chinese Academy of Sciences, Beijing, China

13 <sup>4</sup>Key Laboratory of Land Surface Process and Climate Change in Cold and Arid Regions,  
14 Cold and Arid Regions Environmental and Engineering Research Institute, Chinese  
15 Academy of Sciences, Lanzhou, China

16

17 Corresponding author:

18 Lan Cuo

19 Phone: 086-010-84097091

20 Fax: 086-010-84097079

21 Email: [lancuo@itpcas.ac.cn](mailto:lancuo@itpcas.ac.cn)

22

23



24 **Abstract** Changes in plant functional types (PFTs) have important implications for both  
25 climate and water resources. Still, little is known about whether and how PFTs have  
26 changed over the past decades on the Northern Tibetan Plateau (NTP) where several of  
27 the top largest rivers in the world are originated. Also, the relative importance of  
28 atmospheric conditions versus soil physical conditions in affecting PFTs is unknown on  
29 the NTP. In this study, we used the improved Lund-Potsdam-Jena Dynamic Global  
30 Vegetation Model to investigate PFT changes through examining the changes in foliar  
31 projective coverages (FPCs) during 1957-2009 and their responses to changes in root  
32 zone soil temperature, soil moisture, air temperature, precipitation and CO<sub>2</sub>  
33 concentrations. The results show spatially heterogeneous changes in FPCs across the  
34 NTP during 1957-2009, with 34% (13%) of the region showing increasing (decreasing)  
35 trends. Dominant drivers responsible for the observed FPC changes vary with regions and  
36 vegetation types, but overall, precipitation is the major factor in determining FPC  
37 changes on the NTP with positive impacts. Soil temperature increase exhibits small but  
38 negative impacts on FPCs. Different responses of individual FPCs to regionally varying  
39 climate change result in spatially heterogeneous patterns of vegetation changes on the  
40 NTP. The implication of the study is that fresh water resources in one of the world's  
41 largest and most important headwater basins and the onset and intensity of Asian  
42 monsoon circulations could be affected because of the changes in FPCs on the NTP.

43

44 **Keywords:** Plant functional types, foliar projective coverage, dynamic vegetation  
45 modeling, climate change, northern Tibetan Plateau, desertification

46



47 **1. Introduction**

48 Vegetation dynamics can directly affect water, energy and carbon balances in the coupled  
49 land-atmosphere system by responding and providing feedbacks to climate change  
50 (Bonan et al., 1992; Bonan et al., 2003; Rogers et al., 2013; Ahlstrom et al., 2015;  
51 Mengis et al., 2015; Paschalis et al., 2015; Peterman et al., 2015; Sitch et al., 2015). In  
52 recent years, dynamic global vegetation models (DGVMs) coupled with atmospheric  
53 processes have become valuable tools for examining and understanding the interactive  
54 dynamics in carbon, water, and energy exchanges between biosphere and atmosphere.  
55 The representation of dynamic vegetation has also become a key component in the earth  
56 system models since the last decade (Levis et al., 2004; Sato et al., 2007; Hopcroft et al.,  
57 2015). There are many widely used DGVMs that include TRIFFID (Cox, 2001), LPJ  
58 (Sitch et al., 2003), BIOME-BGC (Tatarinov and Cienciala, 2006), CENTURY  
59 (Smithwick et al., 2009), and OCHIDEE (Ciais et al., 2008), just to name a few. Most of  
60 these DGVMs employ the so-called climate envelop approach to control the  
61 redistribution of plant, whereas TRIFFID uses the Lotka-Volterra representation of  
62 competitive ecological processes for plant redistribution (Fisher et al., 2015).

63

64 One common way to describe vegetation in many DGVMs is the adoption of the term  
65 plant functional type (PFT) for classifying plants into discrete groups according to their  
66 ecological, physiological and phylogenetic traits (Cox, 2001; Sitch et al., 2003). In many  
67 of the state-of-the-art hydrological and land surface models, PFT is both an input for  
68 driving the land-atmosphere processes (e.g., Liang et al., 1994; Liang et al., 1996;  
69 Wigmosta et al., 1994) and an output of dynamic vegetation simulations (e.g., Sitch et al.,



70 2003). When climate changes, PFTs may migrate or retreat depending on bioclimatic  
71 limits and availability of water and light (Pearson et al., 2013). For example, Jiang et al.  
72 (2012) examined the Lund-Potsdam-Jena Dynamic Global Vegetation Model (LPJ-  
73 DGVM) simulations and showed that temperate trees were more sensitive to climate  
74 change than boreal trees and perennial C3 grasses, suggesting that anomalous warming in  
75 the northern high latitudes could change the composition of PFTs and cause the  
76 northward migration of temperate trees. Changes in the composition of PFTs due to  
77 climate change could also modify the foliar projective coverage (FPC, the proportion of  
78 ground area that is covered by leaves), an important quantity in determining water,  
79 energy, and C exchange (Weiss et al, 2014; Meng et al., 2015). Given the fact that  
80 evapotranspiration and photosynthesis are closely related to the foliar properties (Swank  
81 and Douglass, 1974; Huber and Iroume, 2001; Zhang et al., 2015), some dynamic  
82 vegetation models use FPC to represent PFT (e.g., Sitch et al., 2003).

83

84 Due to its massive size and high altitude, the Tibetan Plateau (TP) exerts strong influence  
85 on regional and global climate through mechanical and thermal-dynamic forcing (Yanai  
86 et al., 1992; Wang et al., 2008). The TP is characterized by complex terrain,  
87 heterogeneous land surfaces, spatially varying energy and water patterns, diverse  
88 ecosystems and bioclimatic zones (Yeh and Gao, 1979; CAS, 2007). The surface  
89 conditions of the TP, such as snow cover, soil moisture and vegetation all affect the  
90 strength and evolution of the East Asian and South Asian monsoons (Reiter and Gao,  
91 1982; Ye and We, 1998; Zhang et al., 2004; Qiu, 2008). It is also the headwater region  
92 of the major rivers in Asia (Cuo et al., 2014). In particular, the northern TP (NTP; 30-



93 40 °N, 90-105°E) where the Yellow, Yangtze and Mekong Rivers originate, is crucially  
94 important in providing water and other ecosystem services to the plateau itself and the  
95 downstream regions hosting billions of population. Changes in the composition of  
96 different PFTs, and consequently FPCs, could substantially affect surface  
97 evapotranspiration, soil water storage and streamflow (Cuo et al., 2009; Cuo et al., 2013a;  
98 Weiss et al., 2014; Cuo, 2015; Dahlin et al., 2015), and the partition of net radiation into  
99 the sensible and latent heat fluxes, consequently affecting the onset and intensity of south  
100 and east Asian monsoon circulations (Wu et al., 2007; Cui et al., 2015). Although there  
101 are some studies that connect NDVI (Normalized Difference Vegetation Index) and NPP  
102 (Net Primary Production) to precipitation, air temperature, and CO<sub>2</sub> concentrations on the  
103 TP (Zhong et al., 2010; Chen et al., 2012; Piao et al., 2012), very few studies have  
104 examined PFT changes and their relationships with climate for the region (Wang X.,  
105 2011).

106

107 Besides precipitation, air temperature and CO<sub>2</sub> change impacts on the plants, changes in  
108 soil temperature and soil moisture could also affect heterotrophic respiration (litter  
109 decomposition, soil carbon release, etc.) and vegetation root development. Jin et al. (2013)  
110 found that spatial patterns and temporal trends of phenology were parallel with the  
111 corresponding soil physical conditions over the TP, and that 1°C increase in soil  
112 temperature could advance the start of the growing season by 4.6 – 9.9 days. On the TP  
113 where a vast area of seasonally frozen (SFS) and permafrost (PFS) soil exists (Cheng and  
114 Jin, 2013), global warming induced frozen soil degradation (Cuo et al., 2015) could  
115 potentially affect litter decomposition and plant phenology (Jin et al., 2013).



116

117 To date, little is still known about the changes in PFTs or FPC on the NTP in recent  
118 decades, much less the mechanisms behind these changes, largely due to the lack of long-  
119 term observation data and appropriate research tools. This knowledge gap greatly limits  
120 our understanding of TP's vegetation dynamics in response to climate change and the  
121 associated implications in the regional and global water, energy and carbon cycles. This  
122 study aims to fill this knowledge gap by investigating the changes in PFTs on the NTP in  
123 1957-2009 and the underlying mechanisms using a dynamic vegetation model, the LPJ-  
124 DGVM model. Important atmospheric and soil variables that could significantly affect  
125 PFT changes, including precipitation, air temperature, CO<sub>2</sub> concentration, soil  
126 temperature and soil moisture, are examined and their importance is compared using a  
127 dynamic vegetation model.

128

## 129 **2. Methods and data**

### 130 2.1 Study area

131 The NTP lies between 1400 and 6100 m above sea level, with an average elevation of  
132 around 3900 m (Fig. 1). Five large mountains, the Hengduan in the southeast, the  
133 Tanggula in the southwest, the Kunlun in the center, the Arjin in the northwest, and the  
134 Qilian in the north are located on the NTP. Vegetation on the NTP changes from forest in  
135 the southeast to grassland and desert in the northwest, with major vegetation types  
136 including temperate evergreen needleleaf forest, summergreen needleleaf and broadleaf  
137 forest, temperate shrub/grassland, alpine meadow, alpine steppe, sparsely vegetated bare  
138 land and desert. Annual precipitation ranges from 1000 mm in the southeast to less than



139 100 mm in the northwest. Annual air temperature is high in the low elevation (about  
140 15 °C) and low in the high elevation (about -10 °C). Details of the spatial patterns of the  
141 climate elements and their changes on the NTP over the past five decades can be found in  
142 Cuo et al. (2013b).

143

#### 144 2.2 The LPJ model and its parameterizations for the NTP

145 We used the LPJ-DGVM model (Sitch et al., 2003; Gerten et al., 2004; LPJ hereafter) to  
146 simulate vegetation dynamics, C cycle and biogeophysical properties. Vegetation  
147 dynamics in LPJ are driven by the processes of competition for water, light and nutrients  
148 among plant functional types, with different rates of plant carbon assimilation and  
149 allocation, reproduction, and survival. LPJ can simulate photosynthesis, transpiration, soil  
150 organic matter and litter dynamics and fire disturbance at daily time step, and resource  
151 competition, tissue turnover, population dynamics at annual time step. Plant  
152 establishment is determined by bioclimatic limits. Probability of plant mortality is  
153 controlled by the interactions among light competition, low growth efficiency, a negative  
154 carbon balance, heat stress and bioclimatic limits. LPJ couples fast hydrological and  
155 physiological processes with slower ecosystem processes using daily, monthly, and  
156 yearly time scales (Bonan et al., 2003), and has been successfully applied in the  
157 simulation of global and regional vegetation dynamics and large scale PFT distributions  
158 (Smith et al., 2001; Sitch et al., 2003; Gerten et al., 2004; Sitch et al., 2005; Sitch et al.,  
159 2008; Murray, 2014; Steinkamp and Hickler, 2015).

160



161 Six PFTs, temperate needleleaf evergreen trees, temperate broadleaf evergreen trees,  
162 temperate broadleaf summergreen trees, perennial alpine meadow grasses, perennial  
163 alpine steppe grasses, and perennial temperate summergreen scrub/grassland are  
164 compiled and used in the model to represent the major vegetation types on the NTP,  
165 based on physiognomic (tree or herbaceous), bioclimatic (temperate, boreal or alpine),  
166 phenological (evergreen or summergreen), and photosynthetic (C3 or C4) properties of  
167 the plants. The vegetation state of each of the  $0.25^\circ \times 0.25^\circ$  grid cells in LPJ is a mixture  
168 of PFTs that can be distinguished by their FPCs. FPC of an individual PFT, ranging from  
169 0 (zero coverage) to 100 (full coverage), is a function of crown area (for trees only),  
170 individual density and LAI, and is calculated by the Lambert-Beer law (Sitch et al., 2003).  
171 The total FPC of a given space is the sum of the FPCs of all PFTs in that space.  
172  
173 On the NTP, vegetation root system is concentrated in the top 0.4 m depth where soil  
174 undergoes seasonal freezing and thawing cycles. The accuracy of heat and moisture  
175 content representation in the top 0.4 m soil is therefore vital for modeling vegetation  
176 dynamics and C cycle in this region. In this work, LPJ is configured with two soil layers,  
177 0-0.4 m (top layer) and 0.4-1.0 m (bottom layer) below surface, for better accounting for  
178 water and energy states of the top soil layer under repeated freezing and thawing cycles  
179 on the NTP, while at the same time maintaining its computational efficiency for large  
180 scale simulations. Daily temperature of the top soil layer is calculated by linearly  
181 regressing it with daily air temperature. The linear relationship is obtained from five  
182 stations (stars in Fig. 1) where both soil temperature and air temperature observations are  
183 available. These five stations are located in the different parts of the NTP and represent



184 various land cover types (temperate shrub/grassland, alpine meadow, alpine steppe and  
 185 desert) and soil conditions (SFS and PFS). Depending on the stations, the observation  
 186 periods are different. Both monthly and annual soil temperature at stations with  
 187 observation periods greater than 2 years are chosen for the validation of simulated soil  
 188 temperature. The linear regression equations are developed separately for normal (regular  
 189 soil moisture) and desert (dry) soils. For normal soil, daily soil (0-0.4 m depth) and air  
 190 temperature are obtained from Mengyuan (1983-2009, SFS), Maduo (1980-2009, SFS)  
 191 and Wudaoliang (2005-2006, PFS) (Eq. 1). For desert dry soils where monthly soil  
 192 moisture is usually around  $0.1 \text{ m}^3/\text{m}^3$ , daily soil and air temperature are obtained from the  
 193 Mangai (1988-2009) and Lenghu (1980-2009) stations (Eq. 2). Note that desert dry soil  
 194 temperature can change quickly due to the lower thermal capacity of dry air ( $1000 \text{ J K}^{-1}$   
 195  $\text{kg}^{-1}$ ) than that of water ( $4188 \text{ J K}^{-1} \text{ kg}^{-1}$ ), and the slope for desert dry soil is larger than  
 196 that for normal soil. Eqs. (1) and (2) are expressed as:

$$197 \quad ST1 = 0.8753 \times AT + 3.1623, \quad \theta > 0.1; \quad R^2 = 0.94 \quad (1)$$

$$198 \quad ST1 = 1.0873 \times AT + 3.9063, \quad \theta \leq 0.1; \quad R^2 = 0.97 \quad (2)$$

199 where ST1 is daily soil temperature ( $^{\circ}\text{C}$ ) in 0-0.4 m depth, AT is daily air temperature  
 200 ( $^{\circ}\text{C}$ ), and  $\theta$  is total soil moisture ( $\text{m}^3/\text{m}^3$ ).  $R^2$  is coefficient of determination.

201

202 Soil temperature in 0.4–1.0 m depth is assumed to be a lagged exponential function of the  
 203 top layer soil temperature. The equations are as follows:

$$204 \quad ST2 = ST1 + (Ta - ST1) \times e^{-Ts} \quad (3)$$

$$205 \quad Ta = a + b \times \left( N_d - 1 - Ts \times \frac{365}{2\pi} \right) \quad (4)$$



$$206 \quad T_s = \frac{D_2 \times \frac{3}{4}}{\sqrt{Q_d \times 86400 \times 365 / \pi}} \quad (5)$$

$$207 \quad Q_d = \frac{K}{C_s} \quad (6)$$

208 where  $K$  and  $C_s$  are heat conductivity ( $\text{W m}^{-1} \text{K}^{-1}$ ) and volumetric heat capacity ( $\text{J m}^{-3} \text{K}^{-1}$ ), respectively, that are calculated based on the soil mineral and organic content and  
 209 moisture conditions and are updated at a daily time step;  $Q_d$  is heat diffusivity ( $\text{m}^2 \text{s}^{-1}$ );  $D_2$   
 210 is the depth of the second layer;  $N_d$  is the number of days in a year;  $a$  and  $b$  are the linear  
 211 regression coefficients of daily air temperature and the numbers of days in a month,  
 212 respectively, and are updated at a monthly time step. Eq. (4) calculates the lag of the  
 213 thermal change in the second layer soil temperature. The equations employed for the  
 214 second layer soil temperature are the modified version of the originals used in LPJ.  
 215

216

217 Total soil moisture in the top soil layer is obtained from the balance between precipitation  
 218 input, soil evapotranspiration and percolation. Ice and liquid content is calculated based  
 219 on soil temperature. If soil temperature is below  $0^\circ\text{C}$ , soil liquid content is calculated by  
 220 using freezing point depression equation. Ice content is the difference between total soil  
 221 moisture and liquid water content. When soil temperature is greater than  $0^\circ\text{C}$ , soil  
 222 moisture is liquid and ice content is zero. The equations are:

$$223 \quad \theta_l = \varphi \times \left( \frac{-L_f \times ST1}{273.16 \times g \times b_p} \right)^{\frac{-2.0}{n-3}} \quad ST1 < 0 \quad (7)$$

$$224 \quad \theta_i = \theta - \theta_l \quad ST1 < 0 \quad (8)$$

225 where  $\theta$  is total soil moisture and subscripts  $l$  and  $i$  represent liquid and ice, respectively;  
 226  $\varphi$  is soil porosity;  $L_f$  is latent heat of fusion ( $3.337 \times 10^5 \text{ J kg}^{-1}$ );  $g$  is gravitational  
 227 acceleration ( $9.81 \text{ m s}^{-2}$ );  $b_p$  is the bubbling pressure (m); and  $n$  is the exponent in



228 Campbell's equation for hydraulic conductivity. The second layer soil moisture is  
229 calculated using the similar equations, and it is the aggregation of liquid and ice content,  
230 runoff, percolated moisture from the top layer and to the baseflow. Runoff is generated  
231 when liquid soil content is greater than porosity, and percolation is generated when liquid  
232 soil content is greater than soil water holding capacity. Runoff and baseflow are produced  
233 in both soil layers and are removed from soil moisture. Soil moisture observations are  
234 rare on the NTP. Only 1-year observations at 4 permafrost sites are available during the  
235 study period (see Fig. 1) and they are used for soil moisture validation.

236

237 The implementation of the aforementioned processes in the LPJ model requires seven  
238 additional soil parameters for each of the two soil layers: Campbell's exponent  $n$ ,  
239 bubbling pressure  $b_p$ , bulk densities for organic matter and soil mineral, particle densities  
240 for organic matter and soil mineral, and quartz content. Soil porosity  $\phi$  is calculated from  
241 soil bulk density and soil particle density. These parameters are often used in surface  
242 hydrological models for calculating soil hydrological properties (e.g. Liang et al., 1994;  
243 1996; Wigmosta et al., 2004), and are provided for various soil texture types in the LPJ  
244 model. These additional parameters together with the original parameters for soil texture,  
245 soil percolation rates and water holding capacity constitute the new soil parameter sets.  
246 These modifications eliminate the use of fixed heat diffusivity at 0%, 15% and 100%  
247 water content in the original model version, instead here the diffusivity varies with  
248 thermal conductivity and capacity as shown in Eq. (6).

249

250 2.3 Forcing data and observations



251 Forcing data used in the LPJ model include monthly air temperature, precipitation, wet  
252 days, cloud cover amount and annual CO<sub>2</sub> concentrations. Monthly air temperature,  
253 precipitation and wet days, all at 0.25° × 0.25° resolution, were from Cuo et al. (2013b).  
254 Cloud cover data came from the Climate Research Unit of the University of East Anglia  
255 (Mitchell and Jones, 2005) at 0.5° × 0.5° resolution and were regridded to 0.25° × 0.25°  
256 resolution assuming uniform distribution of cloud cover within each 0.5° × 0.5° grid cell.  
257 Annual CO<sub>2</sub> concentrations were obtained from the Mauna Loa Observatory operated by  
258 NOAA (National Oceanic and Atmospheric Administration). Missing CO<sub>2</sub> observations  
259 for 1957 - 1958 were filled in by extrapolating the regression between annual CO<sub>2</sub>  
260 concentrations and the corresponding years. Soil texture data were from the Harmonized  
261 World Soil Data v1.0 (FAO, 2008). Elevation data were from the Shuttle Radar  
262 Topography Mission (SRTM) and were interpolated to the 0.25° × 0.25° grids.

263

#### 264 2.4 Analysis methods

265 To spin up, the LPJ model was run iteratively for 1000 years using the 1957-1986 climate  
266 data and starting from bare ground, a common practice among LPJ users. The purpose of  
267 this long run is to establish ecosystem equilibrium equivalent to the 1957 conditions. Like  
268 earlier studies (e.g., Sitch et al., 2003), we assume that after the 1000-year spinup,  
269 vegetation dynamics, carbon pools, soil thermal and water conditions reach the needed  
270 equilibrium.

271

272 Given the importance of the top 0.4 m soils for vegetation root system on the NTP, we  
273 validate model simulated soil temperature and moisture in this layer against available



274 observations. Deep layer soil temperature and moisture are also evaluated but will not be  
275 shown. Mean, correlation coefficient (R) and root mean square error (RMSE) of monthly  
276 and annual mean soil temperature, as well as monthly soil moisture are examined. FPCs  
277 are used to represent vegetation states and PFTs. The spatial patterns of the simulated  
278 FPCs of dominant PFTs are compared with those of the survey maps compiled by CAS  
279 (2007) and Zheng et al. (2008). Parameters representing the physiological, phenological  
280 and bioclimatic attributes of the six PFTs are adjusted accordingly to obtain a reasonable  
281 match between the simulated pattern and the survey maps. Soil parameters used are from  
282 Cuo et al. (2013a) and model default settings. The calibrated PFT parameters are listed in  
283 Table 1.

284

285 Following model evaluation, we examine the changes in total FPCs and FPCs of  
286 individual PFTs during 1957-2009 in response to climate change. Climate change is  
287 represented by changes in air and 40-cm-deep soil temperatures, 40-cm-deep soil  
288 moisture, precipitation and atmospheric CO<sub>2</sub> concentration. The Mann-Kendall trend  
289 analysis is employed to investigate the FPC trends. Also, the differences between  
290 historical simulation and climate trends removed simulation are examined to identify the  
291 changes in FPCs during the past five decades.

292

293 To investigate the sensitivity of FPCs in each grid cell to changes in soil temperature and  
294 moisture, air temperature, precipitation and CO<sub>2</sub>, six scenarios (S1-S6) are designed  
295 (Table 2). In the baseline scenario (S6), the trends in air temperature, precipitation, wet  
296 day and CO<sub>2</sub> are removed. Soil temperature and moisture respond to atmospheric



297 forcings and they are assumed to have no trends when the trends of atmospheric forcings  
298 are removed. The only difference between S1-5 and S6 scenarios is the introduced  
299 change in one variable while keeping the other variables unchanged. Cloud cover remains  
300 the same for all scenarios. For precipitation, only the amount but not the frequency is  
301 changed. These scenarios bear similarity to what has been identified over the NTP in  
302 recent decades in general in that S1 plus S2, S3, S4 and S5 represent regional frozen soil  
303 degradation, warming, wetting and elevated CO<sub>2</sub> trends, respectively, although the rates  
304 of changes and spatial patterns differ (Cuo et al., 2013b, 2015). Uniform perturbations are  
305 introduced to provide the benchmark for the climate sensitivity comparison across the  
306 region and to derive sensitivity spatial pattern. It is expected that the comparisons  
307 between the paired S1-S6, S2-S6, S3-S6, S4-S6 and S5-S6 scenarios would reveal the  
308 responses of FPC to the changes in soil temperature, soil moisture, air temperature,  
309 precipitation and CO<sub>2</sub>, respectively.

310

311 Using S1-6 scenarios, we examine elasticity (E), a quantity that measures how responsive  
312 a variable is to a changing condition, in order to quantify the degree of the FPC  
313 sensitivity to climate change. Elasticity is calculated as the median of the ratios of  
314 percentage changes in annual FPC to the percentage changes in an annual climate  
315 variable. Positive (negative) E indicates that FPC increases (decreases) with changing  
316 climate variable. Larger E corresponds to higher sensitivity, and when E is zero FPC is  
317 not responding to climate change. In the following, we will use  $E_{ST1}$ ,  $E_{sm1}$ ,  $E_{AT}$ ,  $E_{PRCP}$  and  
318  $E_{CO_2}$  to denote the sensitivity of FPCs to the changes in the top layer soil temperature



319 (ST1) and soil moisture (SM1), air temperature (AT), precipitation (PRCP), and CO<sub>2</sub>,  
320 respectively.

321

### 322 **3. Results**

#### 323 3.1 Evaluations of simulated soil temperature, moisture and FPC

324 Figure 2 shows the simulated and observed monthly soil temperature in the top 0.4 m  
325 depth at Wudaoliang (PFS), Maduo (SFS), Mengyuan (SFS), Mangai (SFS, dry desert  
326 soil) and Lenghu (SFS, dry desert soil). The observations at these sites are also used to  
327 derive the linear regression equations that are then applied over the entire domain. At  
328 Maduo and Mengyuan, the simulated soil temperature matches the observed rather well  
329 in both magnitude and seasonal cycles. At Wudaoliang, the highest station, the simulated  
330 magnitude of the seasonal cycle in soil temperature is larger than the observed while the  
331 opposite is true at Mangai and Lenghu, two dry desert soil stations. Correlation between  
332 the simulations and observations is high ( $R \geq 0.96$ ) across these five stations and RMSE  
333 ranges from 1.40 °C at Maduo to 3.07 °C at Lenghu (Table 3).

334

335 As an independent check, we also compare the simulated and observed monthly soil  
336 temperature of the top soil layer at five other stations whose observations are not used in  
337 deriving the linear regression equations (Fig. 3). These five stations are Xidatan (PFS),  
338 Xinghai (SFS), Zaduo (SFS), Qilian (SFS), and Golmud (SFS, dry desert soil). All five  
339 stations except Xidatan show satisfactory simulations in both magnitude and seasonal  
340 cycles when compared to the observations although Qilian displays underestimation in  
341 the peaks while Golmud exhibits slight overestimation in the first half of the years. At



342 Xidatan, a PFS site, the simulated seasonal cycle is larger than the observed, similar to  
343 Wudaoling as discussed before. It appears that the derived linear regression relationships  
344 may contain some deficiencies at the PFS sites due to the limited observations in the PFS  
345 region. RMSE ranges from 1.32 °C at Zaduo to 3.03 °C at Golmud and 3.21 °C at Xidatan  
346 (Table 3). Correlation between the simulated and observed monthly soil temperature is  
347 higher than 0.97 at these stations (Table 3). For annual soil temperature (Table 3), R is  
348 generally greater than 0.80 and RMSE is generally less than 1.5 °C for all stations except  
349 for Nangqian where RMSE is 4.51 °C and Lenghu where R is 0.53. These analyses  
350 suggest that the modified LPJ model is able to simulate the temporal evolution of the  
351 observed top-layer soil temperature on the NTP with reasonable accuracy.

352

353 For monthly soil moisture, the simulations are largely consistent with the observations in  
354 terms of magnitude and seasonal cycles as reflected by RMSE and R in the range of 0.08  
355 - 0.14 m<sup>3</sup>/m<sup>3</sup> and 0.71 – 0.83, respectively, based on limited observations (Table 4).

356 Slight overestimation of monthly soil moisture is noted at D66 and MS3608 (Table 4).

357

358 Dominant PFTs on the NTP during 1957-2009 simulated by the modified LPJ model is  
359 shown in Fig. 4. The simulated spatial patterns of major PFTs such as perennial alpine  
360 meadow, perennial alpine steppe, barren/sparse grassland and temperate needleleaf  
361 evergreen trees compare favorably with the eco-geographic maps from Zheng et al. (2008)  
362 and the vegetation maps of China at 1:1,000,000 scale by CAS (2007). It should be noted  
363 here that LPJ not only identifies dominant PFTs of each eco-geographic zone but also  
364 creates more diverse PFTs in each zone than those shown by the eco-geographic maps, as



365 can be expected under the complex terrain and diverse climatic conditions of the study  
366 region. Large discrepancies between the simulated and surveyed PFTs exist in the  
367 northeast and southeast of the NTP. For example, the northeastern NTP is dominated by  
368 temperate semi-arid plateau coniferous forest and steppe (HIIC1) according to Zheng et  
369 al. (2008), while it is characterized by alpine meadow mixed with temperate needleleaf  
370 evergreen forests, perennial temperate summergreen scrub/grassland, and alpine steppe in  
371 model simulations. Overall, temperate needleleaf evergreen forest (TNEG hereafter),  
372 perennial alpine meadow (PAMD), perennial alpine steppe (PASP), perennial temperate  
373 summergreen shrub/grassland (TSGS), and barren/sparse grassland prevail over the NTP.  
374

### 375 3.2 Changes in FPCs and climatic factors

376 The Mann-Kendall trends of annual total FPC (the sum of FPCs of all PFTs in one grid  
377 cell), top layer annual soil moisture and temperature, annual precipitation and air  
378 temperature during 1957-2009 are presented in Fig. 5. For FPC, 34% (13%) of the region  
379 shows increasing (decreasing) trends. Decreasing FPCs are found mostly in the northwest  
380 (barren/sparse grassland) and east (TSGS) of the NTP, while increasing FPCs are located  
381 mainly in the northeast and southwest where alpine meadow, steppe and temperate  
382 summergreen shrub/grassland dominate. These change patterns in FPCs are largely  
383 consistent with those of NDVI (Zhong et al., 2010) and NPP (Piao et al., 2012) on the  
384 NTP, further demonstrating LPJ's ability in satisfactorily simulating FPCs and their  
385 changes.  
386



387 Precipitation increases significantly in the northeast but decreases in the northwest and  
388 east of the NTP over the last five decades (Fig. 5). This change pattern in precipitation  
389 largely resembles that of total FPC. Annual changes in the top layer soil moisture also  
390 show a similar spatial pattern to that of precipitation although the trends in soil moisture  
391 are generally small over 79% of the region. Both the top layer soil temperature and air  
392 temperature exhibit warming trends over the entire NTP, with significant trends in the  
393 northwest and the east (Fig. 5). Hence, compared to increasing temperatures, changes in  
394 precipitation appear to play a more important role in determining the spatial patterns of  
395 FPC changes on the NTP. However, over the northwestern and eastern NTP, the  
396 decreasing FPC trends may also be influenced by the warming in addition to the  
397 decreases in precipitation.

398

399 The Mann-Kendall trends of FPCs of the four dominant vegetation types, TNEG, PAMD,  
400 PASP and TSGS, are shown in Fig. 6. TNEG displays patches of increasing FPCs (13%  
401 of the entire area) in the northeast and southeast of the NTP. PAMD (PASP) exhibits  
402 predominantly increasing (decreasing) FPCs within the Qinghai Province, accounting for  
403 45% (44%) of the entire area. FPCs of TSGS increase (13% of the entire area) mainly in  
404 the northeast and decrease (9% of the entire area) mainly in the southeast of the NTP.  
405 Overall, it appears that PAMD has invaded into the domain of PASP over the past 50  
406 years.

407

408 To further investigate possible vegetation migration caused by climate change over the  
409 NTP during 1957-2009, we examine FPC differences between simulations with and



410 without the historical trends in climate variables retained (i.e., Historical – S6 in Table 2).  
411 The results presented in Fig. 7 suggest that by climate change alone, total FPC (Fig. 7a)  
412 would increase by about 20-30% in the northeast and southwest of the NTP but decrease  
413 by less than 30% in some sporadically vegetated locales. FPC decreases in the  
414 northwestern NTP where sparse grassland meets bare land implies an encroachment of  
415 desertification in that region and is especially worrisome. Climate change causes  
416 increases in FPC of TNEG by about 30-60% in most of the eastern NTP (Fig. 7b), and it  
417 decreases FPC of PAMD (30-60%) in the eastern NTP but increases FPC of PAMD (<  
418 30%) in the higher interior of the Qinghai Province, resulting in westward migration of  
419 PAMD (Fig. 7c). On the other hand, as a result of climate change, FPC of PASP  
420 decreases in most of the Qinghai Province but increases (by >30%) in the westernmost  
421 part of the NTP (Fig. 7d). TSGS increases by less than 30% in the northeastern NTP but  
422 decreases by more than 30% in the southeast (Fig. 7e) due to climate change. The spatial  
423 patterns of the FPC changes due to climate change correspond well with those of the FPC  
424 trends (Figs. 5, 6), indicating the dominant role of climate change in governing vegetation  
425 changes and dynamics on the NTP.

426

### 427 3.3 Sensitivity of total FPC to changes in climatic factors

428  $E_{PRCP}$  is positive in 40% of the area and is often larger than 3, meaning that 10%  
429 precipitation increase could lead to more than 3-fold increase in total FPC in warm and  
430 dry places where alpine meadow, barren/sparse grassland, and temperate summergreen  
431 scrub/grassland grow (Fig. 8a). Isolated negative  $E_{PRCP}$  are located mostly in the high  
432 elevation of the southern NTP. About 15% (35%) of the NTP shows positive (negative)



433  $E_{AT}$ . Negative  $E_{AT}$  (-3 - -0.5) is mostly found in the northern NTP (Fig. 8b), indicating  
434 that 1° C warming could lead to 0.5 – 3 fold decrease in total FPC. In the far southwest  
435 (32°-36° N and 90°-93° E) where mean annual air temperature is about -10 °C and where  
436 permafrost soil prevails,  $E_{AT}$  is significantly positive, implying that warming could  
437 dramatically increase FPC by more than 4 folds.  
438  
439 1 °C increase in soil temperature could decrease FPC by up to 4 folds in the northern  
440 NTP (Fig. 8c); however, in the meantime, 10% increase in soil moisture would result in  
441 up to 5 folds of increase in FPC in roughly the same area (Figs. 8d), suggesting that FPC  
442 is highly sensitive to soil moisture changes especially in the climatologically dry  
443 northwest. In the south NTP, FPC seems insensitive to changes in either soil temperature  
444 or soil moisture (Figs. 8c, d).  
445  
446 Positive  $E_{CO_2}$  is slightly more widely distributed than  $E_{PRCP}$  and  $E_{SMI}$  but  $E_{CO_2}$  is in  
447 general much smaller in magnitude than  $E_{PRCP}$  and  $E_{SMI}$  (Fig. 8e). About 62% (4%) of the  
448 cells show positive (negative)  $E_{CO_2}$ . The spatial patterns of elasticity show that foliage  
449 growth in heat or water limited NTP is very sensitive to environmental changes. Figure 8f  
450 depicts the dominant drivers that affect total FPC in each grid cell. Precipitation increase  
451 (light green in Fig. 8f) displays major influence on total FPC in the north with primarily  
452 positive effects (crosses in Fig. 8f). Air temperature increase is less important than  
453 precipitation increase and could exert either positive (crosses in Figs. 8f) or negative  
454 (diamonds in Fig. 8f) effects on total FPC depending on the locations. Generally speaking,  
455 positive (negative) effects due to air temperature increase tend to be clustered in the



456 relatively cold and wet southwest (dry northwest and warm southeast). CO<sub>2</sub> change  
457 impacts are mainly seen over the south and some patchy areas of the north with mixed  
458 positive and negative effects. Compared to the other environmental variables, ST1 and  
459 SM1 do not emerge as the dominant factors for FPC changes, indicating that frozen soil  
460 degradation related to soil temperature and moisture changes is not as important as  
461 changes in precipitation, air temperature and CO<sub>2</sub> for FPC.

462

#### 463 3.4 Sensitivity of the FPC of individual PFTs to changes in climatic factors

464 The FPC of TNEG increases by 1.6-fold on average in response to 10% precipitation  
465 increase in the eastern NTP (about 17% of the entire area, Fig. 9a, Table 5). The FPC of  
466 PAMD increases in 51% of the area by more than 1.2-fold in the east, north and south of  
467 the Qinghai Province, but decreases in 5% of the entire area by about 1-fold in the bare  
468 and sparse grassland and by about 5-fold in several cells in the eastern and southern NTP  
469 as precipitation increases by 10%. The FPC of PASP decreases in the northeast and south  
470 of the Qinghai Province (24% of the region, Table 5) by about 1-fold, but increases in the  
471 northwest desert region of the Qinghai Province by 1- to 3-fold (Fig. 9c). More cells  
472 showing positive  $E_{PRCP}$  for PAMD than for PASP indicates that precipitation increase  
473 would benefit PAMD more than PASP. It appears that as precipitation increases, PAMD  
474 takes over PASP in many cells while PASP encroaches the desert area. The FPC of TSGS  
475 decreases in the southeast by about 1.8-fold but increases by 1.1-fold in the northeast of  
476 the NTP with 10% precipitation increases (Fig. 9d). The southeast NTP is not water  
477 limited and hence increasing precipitation has negative impacts in general.

478



479 Large  $E_{AT}$  for TNEG is found primarily in the eastern NTP, with positive (16% of the  
480 cells) and negative (17% of the cells)  $E_{AT}$  occurring side by side (Fig. 9e). With 1 °C air  
481 temperature increase, PAMD shows positive  $E_{AT}$  (about 5) in the southwest where energy  
482 is limited, but negative  $E_{AT}$  (-1 - -5) in the north, east and southeast (Fig. 9f). For PASP,  
483 large and positive  $E_{AT}$  is found predominantly over the westernmost tip of the NTP,  
484 whereas nearly the entire Qinghai Province (59% of the region) corresponds to negative  
485  $E_{AT}$  (Fig. 9g, Table 5), indicating that PASP would decline in general as air temperature  
486 increases. TSGS shows mixed positive and negative  $E_{AT}$  primarily in the northeast and  
487 southeast, respectively (Fig. 9h). For TSGS and TNEG,  $E_{AT}$  is close to zero over nearly  
488 the entire Qinghai Province (Fig. 9, Table 5), because of the bioclimatic restriction of  
489 their establishment.

490

491 Although soil temperature and moisture changes do not contribute significantly to total  
492 FPC changes (Fig. 8f), they do affect individual PFTs in a nearly opposite way which  
493 may have given rise to some cancellation in FPC changes. For example, with the  
494 exception of TNEG, negative  $E_{ST1}$  over the north and positive  $E_{ST1}$  over the southeast for  
495 PAMD, PASP and TSGS correspond respectively to positive and negative  $E_{SM1}$  in the  
496 same areas (Fig. 10), although  $E_{SM1}$  is generally larger in magnitude than  $E_{ST1}$ . For TNEG,  
497 slightly negative  $E_{ST1}$  is located over the east but highly positive  $E_{SM1}$  is seen over the  
498 north (Figs. 10a, 10e). Compared to  $E_{AT}$ ,  $E_{ST1}$  is smaller and varies less spatially (Figs.  
499 10a-d). The majority cells (72-83%) display zero  $E_{ST1}$  for all four PFTs (Table 5),  
500 indicating that soil temperature is not a sensitive element for foliage growth. However,



501 soil moisture increase could reduce the coverage of desert, evidenced by the increase of  
502 FPCs of TNEG, PAMD and PASP in the northwest where desert vegetation dominates.  
503  
504  $E_{CO_2}$  (Figs. 11a-d) exhibits a similar pattern to that of  $E_{PRCP}$  for all four PFTs (Figs. 9a-d).  
505 The numbers of the grid cells with positive, negative and negligible values of  $E_{CO_2}$  and  
506  $E_{PRCP}$  are also identical for each PFT (Table 5). This similarity between  $E_{CO_2}$  and  $E_{PRCP}$   
507 suggests a strong coupling between photosynthesis and water availability on the NTP.

508

#### 509 **4. Discussions**

510 Our analyses suggest that total FPC changes on the NTP are driven by different  
511 mechanisms over different regions. For example, the increases of total FPC in the  
512 southwest during 1957-2009 identified in Figs. 5 and 7a are due to warming induced  
513 increases in alpine meadow and steppe. Over the northeast of the NTP, changes in total  
514 FPC are determined by the balance between precipitation, soil moisture and  $CO_2$  increase  
515 induced expansion (contraction) of temperate needleleaf evergreen forest, perennial  
516 alpine meadow, perennial temperate summergreen scrub/grassland (perennial alpine  
517 steppe) and warming induced decreases in all FPCs. Decreases of total FPC in the  
518 northwestern NTP are related to the negative effects of warming and drying (Fig. 5) on  
519 the growth of alpine meadow and steppe which apparently overwhelms the positive  
520 effects of  $CO_2$  increase. In the southeast, changes in total FPC are generally small, likely  
521 because of the thriving TNEG growth induced by the increase of temperature,  
522 precipitation and  $CO_2$  cancelled by the decline of PAMD because of warming, and  
523 decreased TSGS due to wetting and  $CO_2$  increase. Similarly, in the central region, PAMD



524 and PASP respond oppositely to the changes in precipitation, air temperature, soil  
525 moisture and CO<sub>2</sub>, and as a result total FPC shows little change.  
526  
527 Different regions of the NTP are characterized by distinctive climatic features, and hence  
528 vegetation growth in those regions is limited by varying climatic factors. For example,  
529 warming and wetting in the southwest of the NTP make it more suitable for alpine  
530 meadow and steppe to grow. On the other hand, the northwestern NTP has very limited  
531 annual precipitation (<100 mm), and the warming could make it even drier (as observed  
532 during the recent decades, see Fig. 5), posing an increasing challenge for plant growth.  
533 As climate changes, bioclimatic zones will change accordingly.  
534  
535 Another noteworthy finding is that as soil temperature increases across the region, there  
536 are more grid cells showing decreasing (14%) than increasing (5%) top layer annual soil  
537 moisture (Fig. 5). The rise in soil temperature on the NTP increases liquid soil moisture  
538 during cold months because of the increased soil thawing but decreases liquid soil  
539 moisture during warm months because of the enhanced soil evaporation in shallow soil  
540 layers (Cuo et al., 2015). Clearly, the decrease in top layer soil moisture in the warm  
541 growing season could negatively impact vegetation growth in the already dry area and  
542 could accelerate desertification unless the lost moisture can be replenished by increasing  
543 precipitation. In the northern NTP, the negative effects of top layer soil temperature  
544 increases on vegetation growth may also serve as an indication of the consequences of  
545 frozen soil degradation that is happening on the NTP (Cuo et al., 2015).  
546



547 On the NTP, decreased (increased) vegetation growth in the northwest (southwest and  
548 northeast) will result in reduction (enhancement) in roughness length and increase  
549 (decrease) in albedo, changes in stomatal resistance, etc. These changes in biogeophysical  
550 properties over the region will feedback to the momentum and carbon exchange, water  
551 and energy balances and will undoubtedly affect large scale circulations such as the onset  
552 and intensity of South and East Asia monsoons (Wu et al., 2007; Shi & Liang, 2014; Cui  
553 et al., 2015; He et al., 2015), thereby affecting the regional and global climate.

554

555 To the authors' knowledge, this work is the first of its kind in that a state-of-the-art  
556 dynamic vegetation model is applied over the NTP for examining the impacts of both  
557 atmospheric conditions and soil physical conditions on plant coverages, and shows that  
558 atmospheric conditions dominate over the soil physical conditions in affecting the FPC  
559 change. This is highly relevant and timely given the fact that the Tibetan Plateau is  
560 experiencing warming and frozen soil degradation. Also, the output of time series  
561 vegetation type maps can be used in hydrological models to further investigate land cover  
562 change impacts on hydrological processes in the region where major Asian rivers are  
563 originated but where such long term time series land cover maps do not exist. Clearly,  
564 understanding the vegetation changes and the underlying mechanisms over the TP is the  
565 first step towards an understanding of the change impacts of TP's surface conditions on  
566 water resources, hydrological cycles and climate at regional and global scales.

567

568 In this study, the role of CO<sub>2</sub> in FPC changes is discussed solely in the context of  
569 photosynthesis. However, CO<sub>2</sub> is a greenhouse gas and increasing CO<sub>2</sub> concentrations



570 have been credited as one of the primary driving forces behind the global warming.

571 Without utilizing a fully coupled dynamic atmosphere-land surface-vegetation model it

572 appears to be rather difficult to separate the effects of CO<sub>2</sub> between photosynthesis

573 related and greenhouse gas related.

574

## 575 **5. Conclusions**

576 In summary, this study documents the changes in PFTs represented by FPCs on the NTP

577 during the past five decades and the possible mechanisms behind those changes through

578 examining the responses of PFTs to changes in climate variables of precipitation, air

579 temperature, atmospheric CO<sub>2</sub> concentrations, 40-cm-deep soil temperature and moisture.

580 Among the five variables, precipitation is found to be the major factor influencing the

581 total vegetation coverage positively, while root zone soil temperature is the least

582 important one with negative impacts. About 34% of the NTP exhibits increasing total

583 FPC trends compared to 13% with decreasing trends during 1957-2009. Individual PFTs

584 respond differently to the changes in the five climate variables. The different responses of

585 individual PFTs to climate change give rise to spatially varying patterns of vegetation

586 change. Spatially diversified changes in vegetation coverage on the NTP are the result of

587 changes in heterogeneous climatic conditions in the region, competitions among various

588 PFTs for energy and water, and regional climate-determined bioclimatic restrictions for

589 the establishment of different PFTs. The effects of the climate change induced regional

590 plant functional type changes on water resources and hydrological cycles in one of the

591 world's largest and most important headwater regions, on the partition of sensible and

592 latent heat fluxes, and hence on the onset and intensity of south and east Asian monsoon



593 circulations should be examined further.

594

#### 595 **Acknowledgement**

596 This study is supported by the National Basic Research Program (grant 2013CB956004),

597 by the National Natural Science Foundation of China (grant 41190083), and by the

598 Hundred Talent Program granted to Lan Cuo by the Chinese Academy of Sciences. The

599 National Center for Atmospheric Research (NCAR)'s Advanced Study Program (ASP) is

600 also acknowledged for providing partial funding for this work.

601

#### 602 **References**

603 Ahlstrom, A., Xia, J., Arneeth, A., Luo, Y., and Smith, B.: Importance of vegetation

604 dynamics for future terrestrial carbon cycling, *Environmental Research Letters*, 10,

605 054019, 2015.

606 Bonan, G.B., Pollard, D., and Thompson, S.L.: Effects of boreal forest vegetation on

607 global climate. *Nature*, 359, 716–718, 1992.

608 Bonan, G., Levis, S., Sitch, S., et al.: A dynamic global vegetation model for use with

609 climate models: concepts and description of simulated vegetation dynamics,

610 *Global Change Biology*, 9, 1543-1566, 2003.

611 Ciais, P., Schelhaas, M.J., Zaehle, S., Piao, S.L., Cescatti, A., Liski, J., Luysaert, S.,

612 LeMaire, G., Schulze, E.D., Bouriaud, O., et al.: Carbon accumulation in European

613 forests. *Nature Geoscience* 1 (7), 425–429, 2008.



- 614 Chen, Z.Q., Shao, Q.Q., Liu, J.Y., and Wang, J.B.: Analysis of net primary productivity  
615 of terrestrial vegetation on the Qinghai-Tibet Plateau, based on MODIS remote  
616 sensing data, *Science China: Earth Sciences*, 55, 1306-1312, 2012.
- 617 Cheng, G. and Jin, H.: Permafrost and groundwater on the Qinghai-Tibet Plateau and in  
618 northeast China, *Hydrogeology Journal*, 21, 5-23, 2013.
- 619 Chinese Academy of Sciences (CAS): Vegetation Map of the People's Republic of China  
620 (1:1000000), 2007.
- 621 Cox, P.M.: Description of the TRIFFID dynamic global vegetation model. Hadley Centre  
622 Technical Note 24: 1–16, 2001.
- 623 Cui, Y., Duan, A., Liu, Y., and Wu, G.: Interannual variability of the spring atmospheric  
624 heat source over the Tibetan Plateau forced by the North Atlantic SSTA, *Climate  
625 Dynamic*, 45, 1617-1634, 2015.
- 626 Cuo, L., Lettenmaier, D.P., Alberti, M., and Richey, J.: Effects of a century of land cover  
627 and climate change on hydrology in Puget Sound, Washington, *Hydrological  
628 Processes*, 23, 907-933, 2009.
- 629 Cuo, L., Zhang, L., Gao, Y., Hao, Z., and Cairang, L.: The impacts of climate change and  
630 land cover transition on the hydrology in the Upper Yellow River basin, China,  
631 *Journal of Hydrology*, 502, 37-52, 2013a.
- 632 Cuo, L., Zhang, Y., Wang, Q., Zhang, L., Zhou, B., Hao, Z., and Su, F.: Climate change  
633 on the northern Tibetan Plateau during 1957-2009: spatial patterns and possible  
634 mechanisms, *Journal of Climate*, 26(1), 85-109, 2013b.



- 635 Cuo, L., Zhang, Y., Zhu, F., and Liang, L.: Characteristics and changes of streamflow on  
636 the Tibetan Plateau: A review, *Journal of Hydrology: Regional Studies*, 2, 49-68,  
637 2014.
- 638 Cuo, L., Zhang, Y., Bohn, T.J., Zhao, L., Li, J., Liu, Q., and Zhou, B. Frozen soil  
639 degradation and its effects on surface hydrology in the northern Tibetan Plateau,  
640 *Journal of Geophysical Research-Atmosphere*, 120, 8276-8298, 2015.
- 641 Cuo, L.: Land use/cover change impacts on hydrology in large river basins: a review. In  
642 *Terrestrial Water Cycle and Climate Change: Natural and Human-Induced*  
643 *Impacts* (eds Q. Tang and T. Oki). American Geophysical Union (AGU)  
644 Geophysical Monograph Series. 2016, (accepted).
- 645 Dahlin, K.M., Fisher, R.A., and Lawrence, P.J.: Environmental drivers of drought  
646 deciduous phenology in the community land model, *Biogeosciences*, 12, 5061-  
647 5074, 2015.
- 648 Fisher, R.A., Muszala, S., Versteinstein, M., Lawrence, P., Xu, C., McDowell, N.G., Knox,  
649 R.G., Koven, C., Holm, J., Rogers, B.M., Spessa, A., Lawrence, D., and Bonan, G.:  
650 Taking off the training wheels: the properties of a dynamic vegetation model  
651 without climate envelopes, *CLM4.5(ED)*, *Geoscience Model Development*, 8,  
652 3593-3619, 2015.
- 653 Gerten, D., Schaphoff, S., Haberlandt, U., Lucht, W., and Sitch, S.: Terrestrial vegetation  
654 and water balance-hydrological evaluation of dynamic global vegetation model,  
655 *Journal of Hydrology*, 286, 249-270, 2004.



- 656 He, B., Wu, G., Liu, Y. and Bao, Q.: Astronomical and hydrological perspective of  
657 mountain impacts on the Asian summer monsoon, *Scientific Reports*, 5, 17586,  
658 2015.
- 659 Hopcroft, P.O., and Valdes, P.J.: Last glacial maximum constraints on the earth system  
660 model HadGEM2-ES, *Climate Dynamics*, 45, 1657-1672, 2015.
- 661 Huber, A., and Iroume, A.: Variability of annual rainfall partitions for different sites and  
662 forest covers in Chile, *Journal of Hydrology*, 248, 78-92, 2001.
- 663 Jiang, Y., Zhuang, Q., Schaphoff, S., Sitch, S., Sokolov, A., Kicklighter, D., and Melillo,  
664 J.: Uncertainty analysis of vegetation distribution in the northern high latitudes  
665 during the 21<sup>st</sup> century with a dynamic vegetation model, *Ecology and Evolution*,  
666 2(3), 593-614, 2012.
- 667 Jin, Z., Zhuang, Q., He, J., Luo, T., and Shi, Y.: Phenology shift from 1989 to 2008 on  
668 the Tibetan Plateau: an analysis with a process-based soil physical model and  
669 remote sensing data, *Climatic Change*, 119, 435-449, 2013.
- 670 Levis, S., Bonan, G.B., Vertenstein, M., and Oleson, K.W.: The community land model's  
671 dynamic global vegetation model (CLM-DGVM): technical description and user's  
672 guide. NCAR Techic Note 459, 1–50, 2004.
- 673 Liang, X., Lettenmaier D.P., and Wood, E.F.: A simple hydrologically based model of  
674 land surface water and energy fluxes for general circulation models, *Journal of*  
675 *Geophysical Research* 99 (D7), 14415–14428, 1994.
- 676 Liang, X., Wood, E.F., and Lettenmaier, D.P.: Surface soil moisture parameterization of  
677 the VIC-2l model: evaluation and modification, *Global and Planetary Change* 13,  
678 195–206, 1996.



- 679 Meng, T.T., Wang, H., Harrison, S.P., Prentice, I.C., Ni, J., and Wang, G.: Response of  
680 leaf traits to climatic gradients: adaptive variation versus compositional shifts,  
681 Biogeosciences, 12, 5339-5352, 2015.
- 682 Mengis, N., Keller, D.P., Eby, M., and Oeschle, A.: Uncertainty in the response of  
683 transpiration to CO<sub>2</sub> and implications for climate change, Environmental  
684 Research Letters, 10, 94001-94001, 2015.
- 685 Mitchell, T.D., and Jones, P.D.: An improved method of constructing a database of  
686 monthly climate observations and associated high-resolution grids. International  
687 Journal of Climatology, 25, 693-712, 2005.
- 688 Murray, S.J.: Trends in 20<sup>th</sup> century global rainfall interception as simulated by a  
689 dynamic global vegetation model: implications for global water resources,  
690 Ecohydrology, 7, 102-114, 2014.
- 691 Paschalis, A., Fatichi, S., Katul, G.G., and Ivanov, V.Y.: Cross-scale impact of climate  
692 temporal variability on ecosystem water and carbon fluxes, Journal of Geophysical  
693 Research-Biogeosciences, 120, 1716-1740, 2015.
- 694 Pearson, R.G., Phillips, S.J., Loranty, M.M., Beck, P.S.A., Damoulas, T., Knight, S.J.,  
695 and Goetz, S.J.: Shifts in Arctic vegetation and associated feedbacks under climate  
696 change, Nature Climate Change, doi:10.1038/nclimate1858, 2013.
- 697 Peterman, W., Bachelet, D., Ferschweiler, K., and Sheehan, T.: Soil depth affects  
698 simulated carbon and water in the MC2 dynamic global vegetation model,  
699 Ecological Modelling, 294, 84-93, 2015.
- 700 Piao, S., Tan, K., Nan, H., Ciais, P., Fang, J., Wang, T., Vuichard, N., and Zhu, B.:  
701 Impacts of climate and CO<sub>2</sub> changes on the vegetation growth and carbon balance



- 702 of Qinghai-Tibetan grasslands over the past five decades, *Global and Planetary*  
703 *Change*, 98-99, 73-80, 2012.
- 704 Qiu J.: China: The third pole. *Nature*, 454, 393-396, 2008.
- 705 Reiter, E.R., and Gao, D.Y.: Heating of the Tibet Plateau and movements of the South  
706 Asian high during spring. *Monthly Weather Review*, 110, 1694-1711, 1982.
- 707 Shi, Q., Liang, S.: Surface-sensible and latent heat fluxes over the Tibetan Plateau from  
708 ground measurements, reanalysis, and satellite data, *Atmospheric Chemistry and*  
709 *Physics*, 14, 5659-5677, 2014.
- 710 Rogers, B.M., Randerson, J.T., and Bonan, G.B.: High-latitude cooling associated with  
711 landscape changes from North American boreal forest fires, *Biogeosciences*, 10,  
712 699–718, 2013.
- 713 Sato, H., Itoh, A., and Kohyama, T.: SEIB–DGVM: A new Dynamic Global Vegetation  
714 Model using a spatially explicit individualbased approach, *Ecological Modelling*,  
715 200, 279–307, 2007.
- 716 Sitch, S., Smith, B., Prentice, I.C., Arneth, A., Bondeau, A., Cramer, W., Kaplan, J.O.,  
717 Levis, S., Lucht, W., Sykes, M.T., Thonicke, K., and Venevsky, S.: Evaluation of  
718 ecosystem dynamics, plant geography and terrestrial carbon cycling in the LPJ  
719 dynamic global vegetation model, *Global Change Biology*, 9, 161-185, 2003.
- 720 Sitch, S., Brovkin, V., Von Bloh, W., Van Vuuren, D., and Eickhout, B.: Impacts of  
721 future land cover changes on atmospheric CO<sub>2</sub> and climate, *Global*  
722 *Biogeochemical Cycle*, 19, GB2013, 2005.
- 723 Sitch, S., Huntingford, C., Gedney, N., Levy, P.E., Lomas, M., Piao, S.L., Betts, R., Ciais,  
724 P., Cox, P., Friedlingstein, P., Jones, C.D., Prentice, I.C., and Woodward, F.I.:



- 725 Evaluation of the terrestrial carbon cycle, future plant geography and climate-  
726 carbon cycle feedbacks using five Dynamic Global Vegetation Models (DGVMs),  
727 Global Change Biology, 14, 2015-2039, 2008.
- 728 Sitch, S., Friedlingstein, P., Gruber, N., Jones, S.D., Murray-Tortarolo, G., Ahlstrom, A.,  
729 Doney, S.C., Graven, H., Heinze, C., et al.: Recent trends and drivers of regional  
730 sources and sinks of carbon dioxide, Biogeosciences, 12, 653-679, 2015.
- 731 Smith, B., Prentice, I.C., and Sykes, M.T.: Representation of vegetation dynamics in the  
732 modeling of terrestrial ecosystems: comparing two contrasting approaches within  
733 European climate space, Global Ecology and Biogeography, 10, 621-637, 2001.
- 734 Smithwick, E.A.H., Ryan, M.G., Kashian, D.M., Romme, W.H., Tinker, D.B., and  
735 Turner, M.G.: Modeling the effects of fire and climate change on carbon and  
736 nitrogen storage in lodgepole pine (*Pinus contorta*) stands, Global Change Biology  
737 15 (3), 535–548, 2009.
- 738 Steinkamp, J. and Hickler, T.: Is drought-induced forest dieback globally increasing?  
739 Journal of Ecology, 103, 31-43, 2015.
- 740 Swank, W.T. and Douglass, J.E.: Streamflow greatly reduced by converting deciduous  
741 hardwood stands to pine, Science, 185, 857-859, 1974.
- 742 Tatarinov, F.A., and Cienciala, R.: Application of BIOME-BGC model manage forests 1:  
743 sensitivity analysis. Forest Ecology and Management, 237(1-3), 267-279, 2006.
- 744 Wang, B., Bao, Q., Hoskins, B., Wu, G., and Liu, Y.: Tibetan Plateau warming and  
745 precipitation changes in East Asia, Geophysical Research Letters, 35, L14702,  
746 2008.
- 747 Wang, X., Cheng, G., and Zhong, X.: Assessing potential impacts of climatic change on



- 748 subalpine forests on the eastern Tibetan Plateau, *Climatic Change*, 108, 225-241,  
749 2011.
- 750 Weiss, M., Miller, P.A., van den Hurk, B.J.J.M., et al.; Contribution of dynamic  
751 vegetation phenology to decadal climate predictability, *Journal of Climate*, 27,  
752 8563-8577, 2014.
- 753 Wigmosta, M.S., Vail, L.W., and Lettenmaier, D.P.: A distributed hydrology vegetation  
754 model for complex terrain, *Water Resources Research*, 30 (6), 1665–1679, 1994.
- 755 Wu, G.X., Liu, Y., Wang, T., Wan, R., Liu, X., Li, W., and Liang, X.: The influence of  
756 mechanical and thermal forcing by the Tibetan Plateau on Asian climate. *J*  
757 *Hydrometeorol* 8(4), 770–789, 2007.
- 758 Yanai, M., Li, C., and Song, Z.: Seasonal heating of the Tibetan Plateau and its effects on  
759 the evolution of the summer monsoon, *Journal of Meteorological Society of*  
760 *Japan*, 70, 319–351, 1992.
- 761 Ye, D.Z., and Wu, G.X.: The role of the heat source of the Tibetan Plateau in the general  
762 circulation. *Meteorology and Atmospheric Physics*, 67, 181-198, 1998.
- 763 Yeh, T.C., and Gao, Y.X.: The Meteorology of the Qinghai-Xizang (Tibet) Plateau (in  
764 Chinese). T.-C. Yeh and Y.-X. Gao et al., Eds., Science Press, Beijing, China, 278  
765 pp, 1979.
- 766 Zhang, Y., Li, T., and Wang, B.: Decadal change of the spring snow depth over the  
767 Tibetan Plateau: The associated circulation and influence on the East Asian  
768 summer monsoon. *Journal of Climate*, 17, 2780-2793, 2004.
- 769 Zhang, Y., Wang, X., Hu, R., Pan, Y., and Paradeloc, M.: Rainfall partitioning into  
770 throughfall, stemflow and interception loss by two xerophytic shrubs within a



771 rain-fed re-vegetated desert ecosystem, northwest China, Journal of Hydrology,  
772 527, 1084-1095, 2015.

773 Zheng, D., Yang, Q.Y., Wu, S.H. et al.: Eco-geographical Region System of China.  
774 Beijing: The Commercial Press, 2008. (in Chinese)

775 Zhong, L., Ma, Y., Suhyb, S.M., and Su, Z.: Assessment of vegetation dynamics and their  
776 response to variations in precipitation and temperature in the Tibetan Plateau,  
777 Climatic Change, 103, 519-535, 2010.

778

779

780

781

782

783

784

785

786

787

788

789

790

791

792

793



794 Table 1. Calibrated parameters of plant functional types in the Lund-Potsdam-Jena DGVM model.

Plant functional types	$g_{min}$ (mm/s)	GDDs	GDD <sub>5min</sub>	Int	$W_{s-m}$	RD <sub>0</sub>	TLCO <sub>2</sub> (°C)	TUCO <sub>2</sub> (°C)	TLP (°C)	TUP (°C)	TL <sub>coold</sub> (°C)
Temperate broadleaf evergreen	1.6	400	900	2.5	0.2	0.8	-3	30	15	30	-0.1
Temperate needleleaf evergreen	1.8	300	600	2.7	0.4	0.8	-10	15	5	-1	-15.5
Temperate broadleaf summergreen	1.5	300	700	1.0	0.2	0.8	-3	20	5	20	-10
Perennial alpine meadow	0.05	70	60	0.1	0.2	1.0	-6	15	0	15	-20
Perennial alpine steppe	0.05	10	20	0.1	0.2	1.0	-20	5	-7	5	-25
Temperate scrub grass	0.4	200	500	0.5	0.2	1.0	-10	18	5	18	-10

795 Note:  $g_{min}$ : minimum canopy conductance; GDDs: number of growing degree days to attain full leaf cover; GDD<sub>5min</sub>: 5 °C based minimum degree day; Int: 800  
 796 interception storage;  $W_{s-m}$ : water scalar value at which leaves shed by drought for deciduous plant; RD<sub>0</sub>: fraction of roots in the upper soil layer (0-40 cm);  
 797 TLCO<sub>2</sub>: lower temperature limit for CO<sub>2</sub>; TUCO<sub>2</sub>: upper temperature limit for CO<sub>2</sub>; TLP: lower temperature limit for photosynthesis; TUP: upper temperature  
 798 limit for photosynthesis; TL<sub>coold</sub>: lower limit of the coldest monthly mean temperature.

801 Table 2. Scenarios used for examining the FPC sensitivity to climate elements.

Scenarios	Variables changed	Changed amount
S1	40-cm-deep daily soil temperature (ST1)	+1 °C
S2	40-cm-deep daily soil moisture (SM1)	+10%
S3	Monthly air temperature (AT)	+1 °C
S4	Monthly precipitation (PRCP)	+10%
S5	Annual CO <sub>2</sub>	+10%
S6	AT, PRCP, wet day, CO <sub>2</sub>	Trends removed
Historical	-	-

802  
 803  
 804  
 805  
 806  
 807  
 808



809 Table 3. Statistics of the observed and simulated monthly and annual mean soil  
 810 temperature in 0-40 cm depth. The observations end in 2009 for all stations except  
 811 for Wudaoliang and Xidatan for which the observations end in 2006. R: correlation  
 812 coefficient; RMSE: root mean square error.

Stations	Start	Latitude	Longitude	Elevation (m)	Obs. (°C)	Sim. (°C)	R	RMSE (°C)
Monthly								
Wudaoliang	2005	35.217	93.083	4612.2	-1.74	-1.57	0.96	2.89
Maduo	2004	34.917	98.217	4272.3	2.13	0.91	0.99	1.40
Mengyuan	2004	37.383	101.617	2938.0	5.29	6.05	0.99	1.67
Mangai	2004	38.250	90.850	2944.8	8.81	9.70	1.00	2.68
Lenghu	2004	38.750	93.333	2770.0	7.50	6.99	1.00	3.07
Xinghai	2004	35.583	99.983	3323.2	5.71	5.27	0.99	1.40
Zaduo	2004	32.900	95.300	4066.4	5.67	5.31	0.99	1.32
Qilian	2004	38.183	100.250	2787.4	5.88	4.70	1.00	2.08
Xidatan	2005	35.717	94.133	4538.0	-0.45	-0.70	0.98	3.21
Golmud	2004	36.417	94.900	2807.6	9.16	11.89	0.99	3.03
Annual								
Mangai	1989	38.250	90.850	2944.8	8.17	8.15	0.82	0.53
Lenghu	1981	38.750	93.333	2770.0	7.56	7.82	0.53	0.70
Delingha	1982	37.367	97.367	2981.5	7.23	7.85	0.94	0.67
Gangcha	1981	37.333	100.133	3345.0	3.59	3.89	0.90	0.38
Mengyuan	1984	37.383	101.617	2938.0	4.69	5.63	0.93	0.97
Germud	1977	36.417	94.900	2807.6	8.53	10.48	0.68	2.08
Qiabuqia	1983	36.267	100.617	2835.0	7.89	8.23	0.82	0.67
Xining	1962	36.717	101.750	2295.2	9.02	9.73	0.67	0.90
Minhe	1994	36.317	102.850	1813.9	11.22	11.57	0.61	0.74
Xinghai	1993	35.583	99.983	3323.2	5.48	5.23	0.80	0.36
Qumalai	1984	34.133	95.783	4175.0	3.05	1.46	0.90	1.63
Maduo	1981	34.917	98.217	4272.3	1.47	0.88	0.87	0.75
Dari	1981	33.750	99.650	3967.5	3.03	2.20	0.87	0.90
Henan	1982	34.733	101.600	3670.0	3.85	3.83	0.90	0.79
Jiuzhi	1979	33.433	101.483	3628.5	4.58	3.84	0.90	0.79
Nangqian	1994	32.200	96.483	3643.7	8.63	4.13	0.92	4.51

813  
 814 Table 4. Statistics of the first layer (0-40 cm) monthly soil moisture. The observation  
 815 period is August 1997 – September 1998.

Stations	Latitude	Longitude	Elev. (m)	Mean Obs. (m <sup>3</sup> /m <sup>3</sup> )	Mean Sim. (m <sup>3</sup> /m <sup>3</sup> )	R	RMSE (m <sup>3</sup> /m <sup>3</sup> )
Amdo	32.25	91.63	4700	0.14	0.15	0.76	0.10
D66	35.52	93.78	4600	0.08	0.13	0.83	0.10
MS3608	31.24	91.78	4610	0.16	0.20	0.80	0.14
Tuotuohe	34.22	92.43	4353	0.12	0.13	0.71	0.08

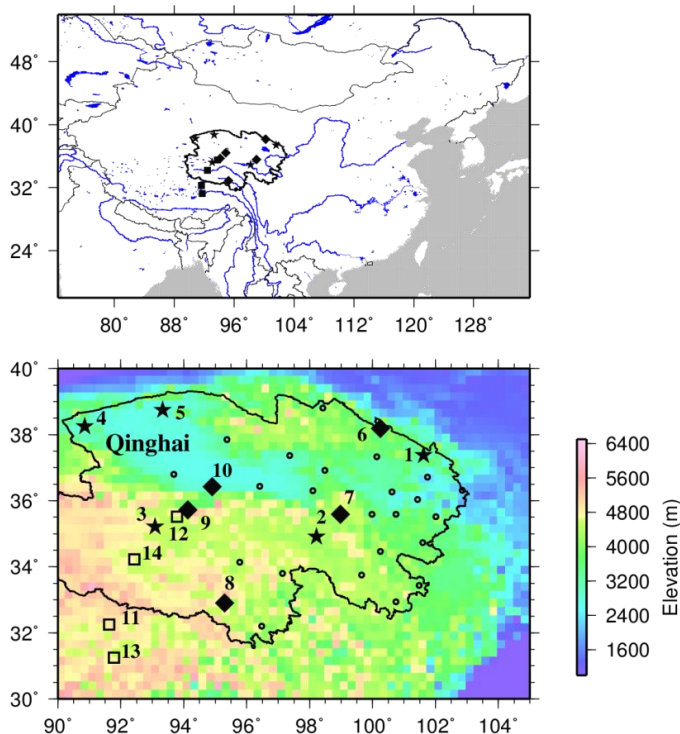
816 Table 5. Numbers of the cells that display positive (+), negative (-) and non or  
 817 negligible (n) elasticity for the four major plant functional types with precipitation



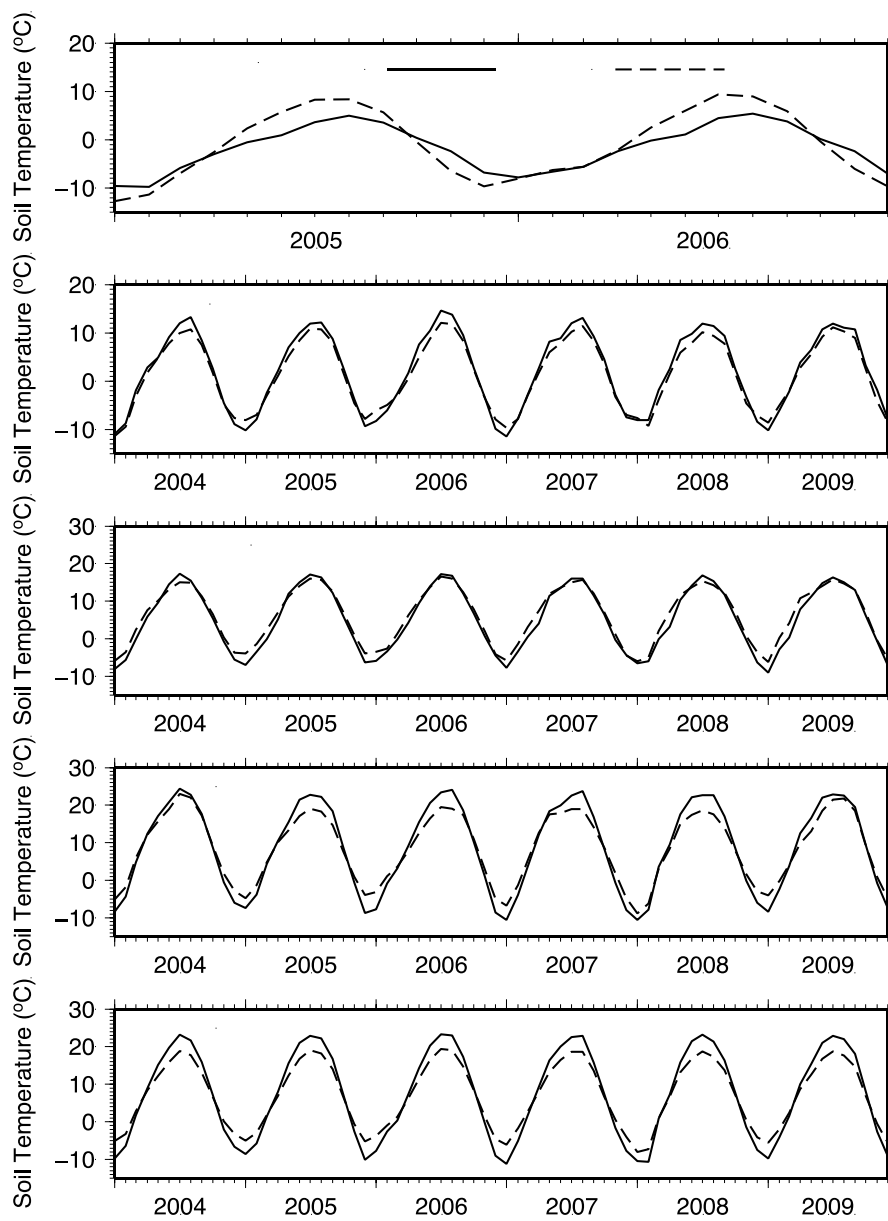
818 increased by 10% (Prpc 10%), air temperature increased by 1 °C (AT+1), top layer  
 819 soil temperature increased by 1 °C (ST+1), top layer soil moisture increased by 10%  
 820 (SM 10%), and CO<sub>2</sub> concentrations increased by 10% (CO<sub>2</sub> 10%). There are 2052  
 821 grid cells in total. TNEG: temperate needleleaf evergreen, PAMD: perennial alpine  
 822 meadow, PASP: perennial alpine steppe, TSGS: temperate summer green  
 823 grass/shrub

Scenarios	Cell signs	TNEG	PAMD	PASP	TSGS
Prpc 10%	+	368	1064	530	184
	-	68	112	509	317
	n	1616	876	1013	1551
AT+1	+	216	761	132	348
	-	364	711	1226	237
	n	1472	580	694	1467
ST+1	+	19	39	2	254
	-	327	522	421	165
	n	1706	1491	1629	1633
SM 10%	+	701	1012	418	142
	-	36	72	492	340
	n	1315	968	1142	1570
CO <sub>2</sub> 10%	+	280	1302	590	185
	-	99	64	557	336
	n	1673	686	905	1531

824  
 825  
 826  
 827  
 828  
 829  
 830  
 831  
 832  
 833  
 834  
 835  
 836  
 837  
 838  
 839  
 840  
 841  
 842  
 843  
 844  
 845  
 846  
 847

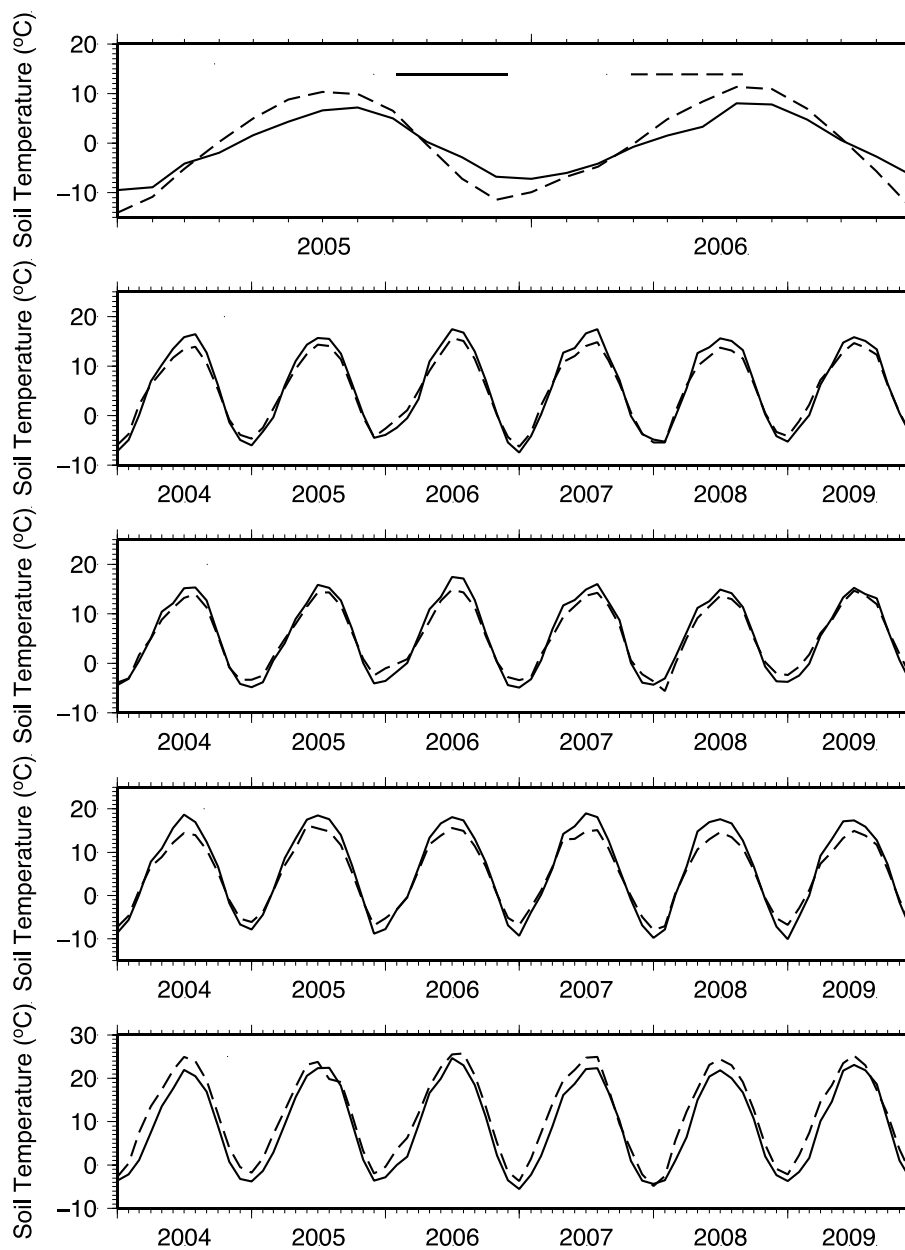


848  
 849 Figure 1. Geographic locations of the study domain and the stations. Black lines  
 850 outline the boundary of the Qinghai Province. Stars represent the stations whose  
 851 observations are used to develop the linear regression relationships between daily  
 852 air temperature and 0-40cm depth daily soil temperature. Stations denoted as  
 853 diamonds are for monthly soil temperature evaluation and circles are for annual soil  
 854 temperature evaluation. The stations are: 1: Mengyuan; 2: Maduo; 3: Wudaoliang; 4:  
 855 Mangai; 5: Lenghu; 6: Qilian; 7: Xinghai; 8: Zadu; 9: Xidatan; 10: Germud; 11: Amdo;  
 856 12: D66; 13: MS3608; 14: Tuotuohe. Among the stations, Wudaoliang, Xidatan,  
 857 Amdo, D66, MS3608 and Tuotuohe are permafrost soil sites and all others are  
 858 seasonally frozen soil sites. Stations 1-10 and circles were used for soil temperature  
 859 validation while stations 11-14 (empty squares) were used for soil moisture  
 860 validation.  
 861



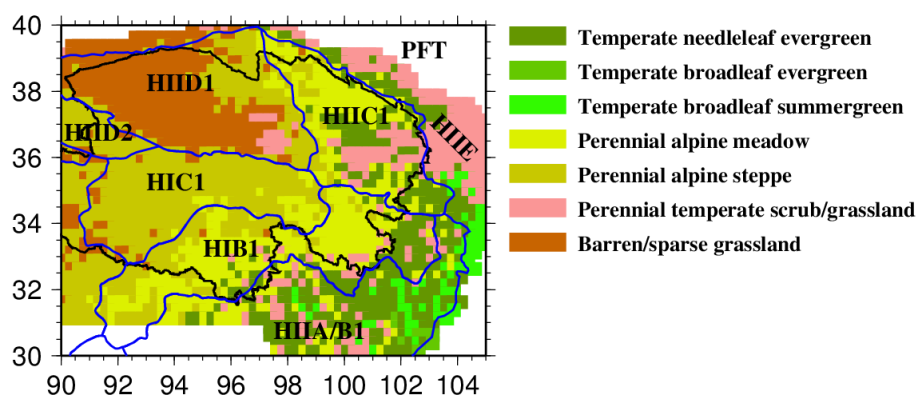
862  
863  
864

Figure 2. Simulated and observed monthly soil temperature at 5 calibration sites.

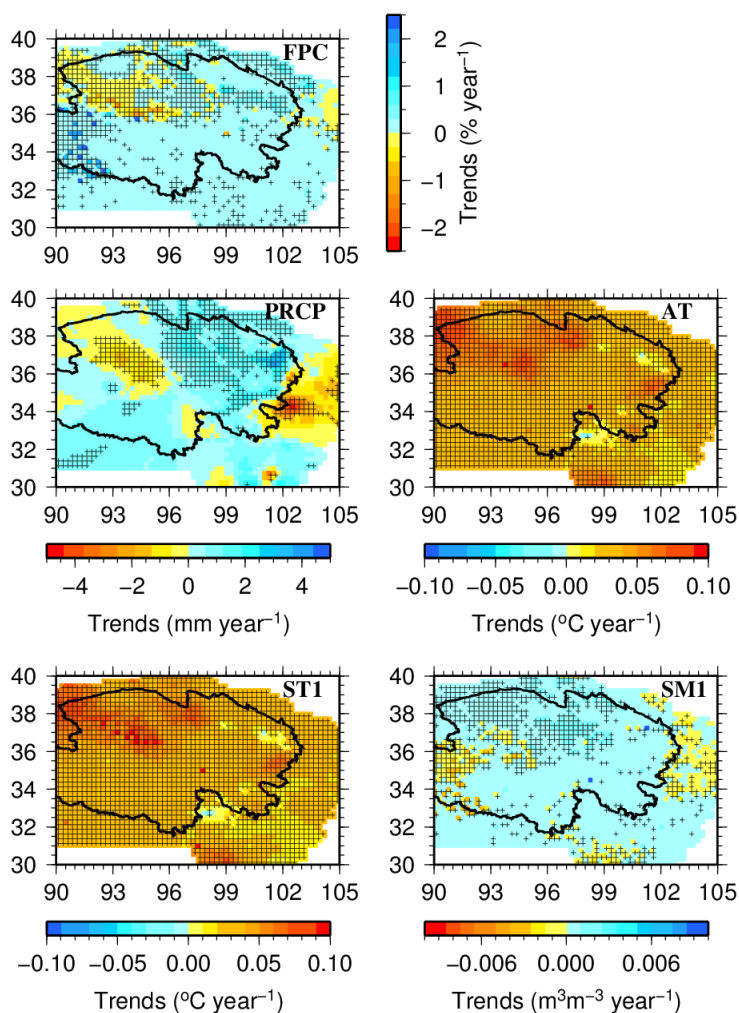


865  
866  
867

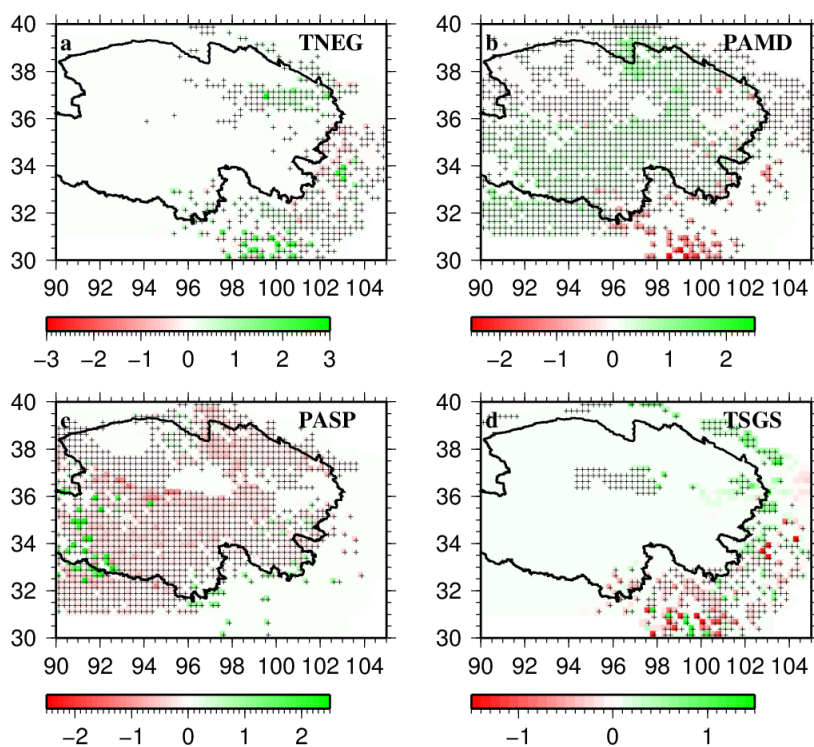
Figure 3. Simulated and observed monthly soil temperature at 5 evaluation sites.



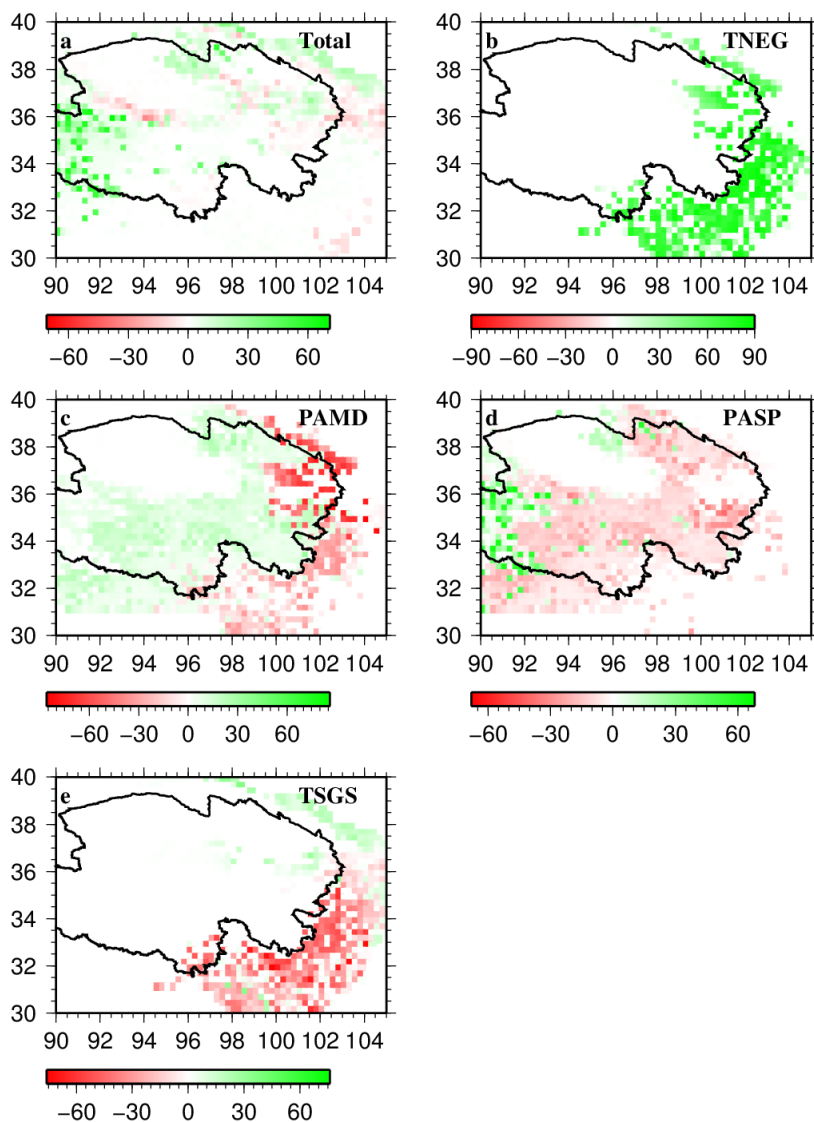
868  
 869 Figure 4. Eco-geographic regions from Zheng et al. (2008) (blue lines) and the LPJ  
 870 simulated dominant plant functional types represented by foliar projective covers  
 871 (FPCs) under full leaf during 1957-2009. The eco-geographic regions are: HIIIC1:  
 872 plateau temperate semi-arid high mountain and basin coniferous forest and steppe  
 873 region; HIID1: plateau temperate arid desert region; HIID2: plateau temperate arid  
 874 desert region; HIC1: plateau sub-cold semi-arid alpine meadow-steppe region; HIB1:  
 875 plateau sub-cold sub-humid alpine shrub-meadow region; HIIA/B1: plateau  
 876 temperate humid/sub-humid high mountain and deep valley coniferous forest  
 877 region; and HIE: temperate shrub grass-desert region. Black line outlines the  
 878 Qinghai Province.  
 879  
 880



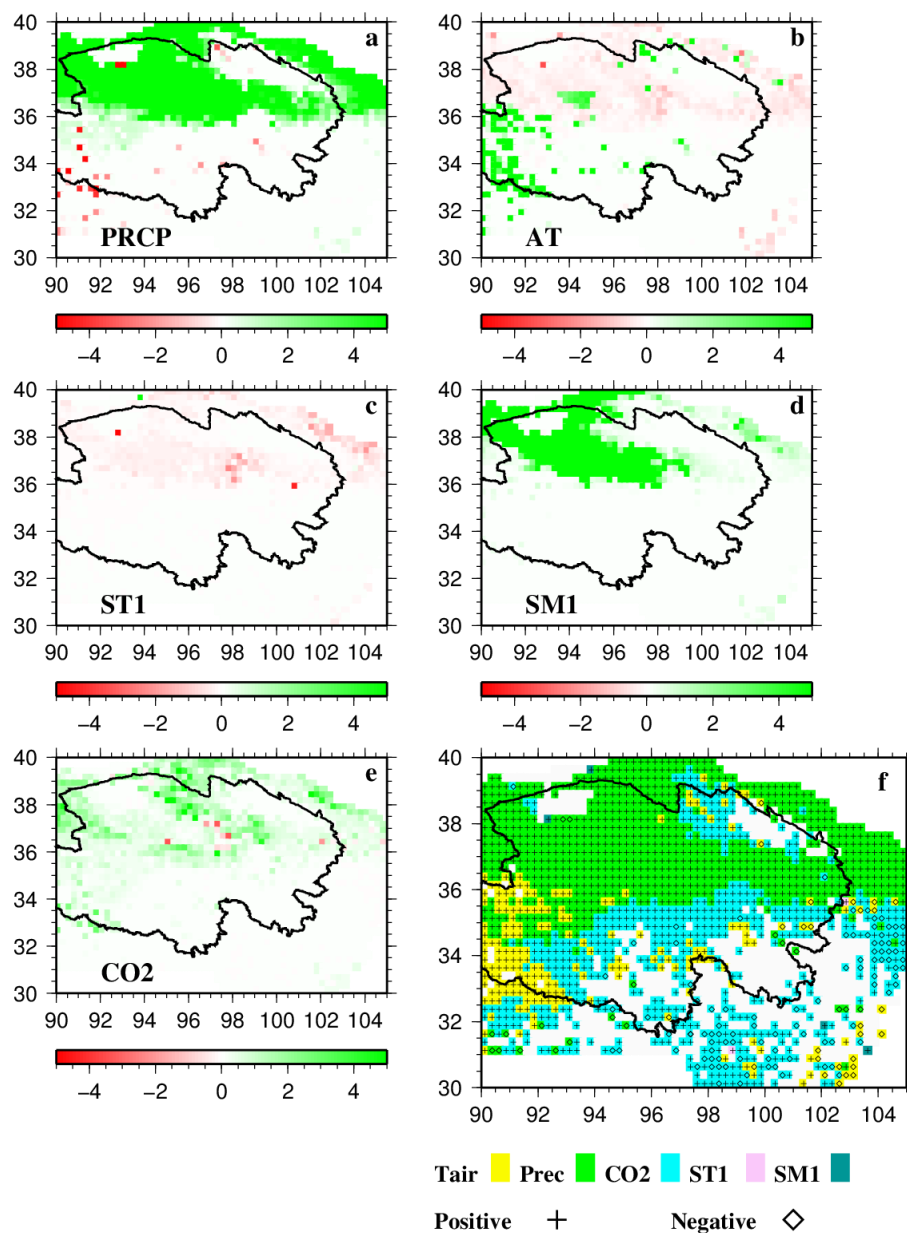
881  
882 Figure 5. Mann-Kendall trends of simulated annual total FPC, 0-40 cm depth soil  
883 temperature (ST1), 0-40 cm depth soil moisture (SM1), and observed precipitation  
884 (PRCP) and air temperature (AT).  
885



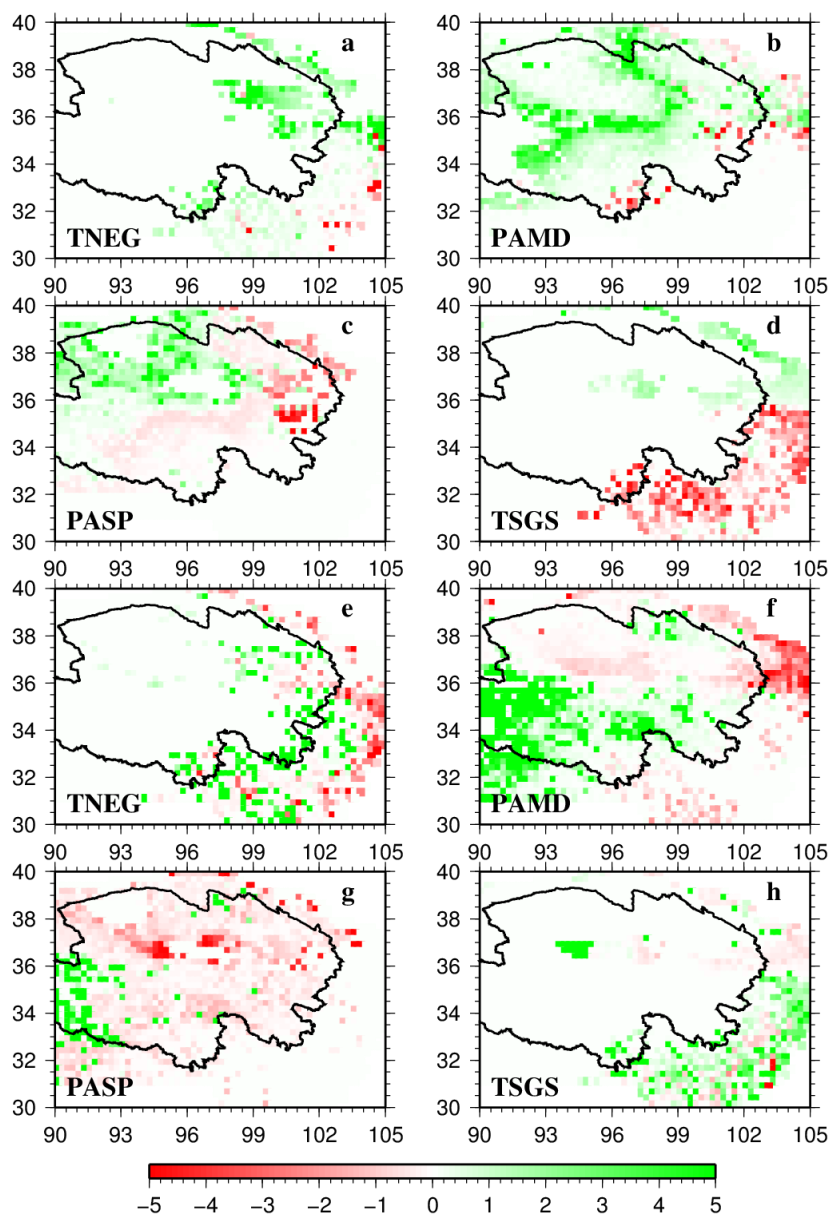
886  
887 Figure 6. Simulated Mann-Kendall trends of individual FPCs in 1957-2009. TNEG:  
888 Temperate needleleaf evergreen, PAMD: perennial alpine meadow, PASP: perennial  
889 alpine steppe, TSGS: temperate summer green scrub/grassland.  
890  
891



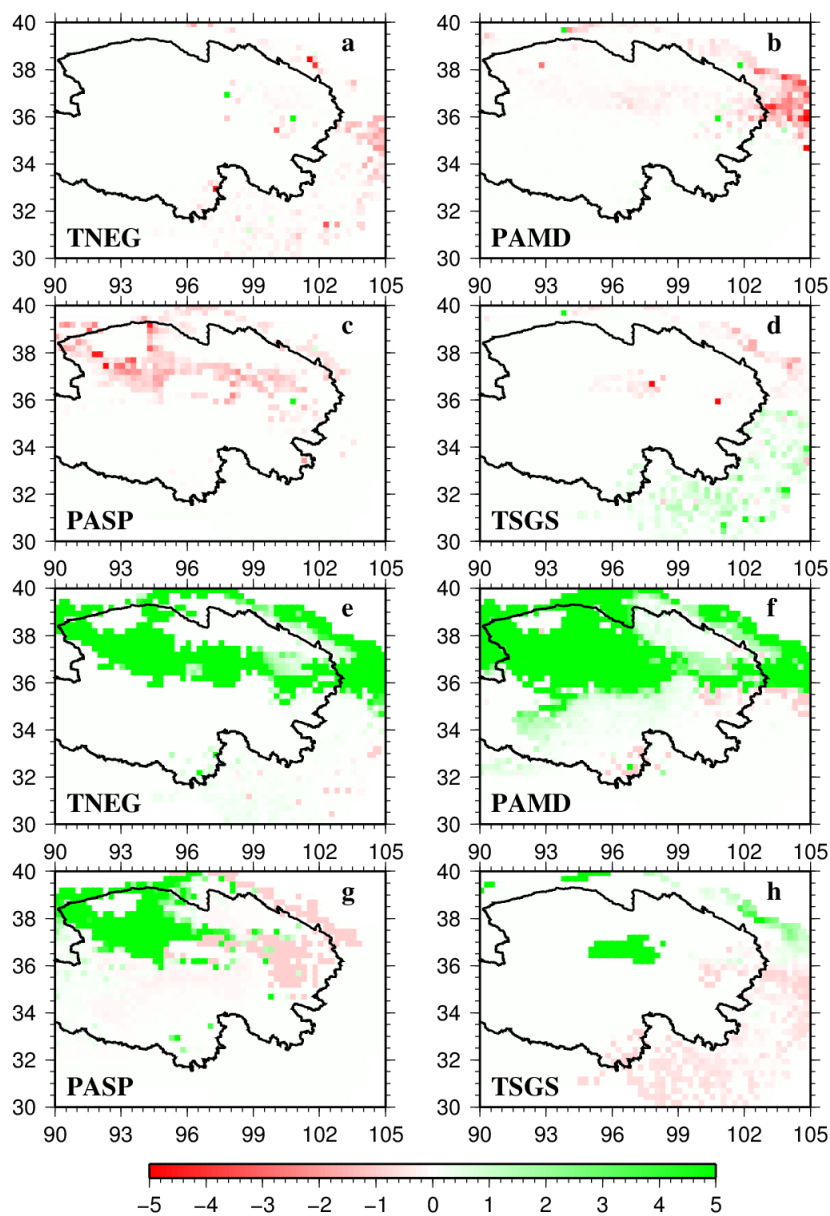
892  
893 Figure 7. Differences (%) in total FPC and individual FPCs between historical  
894 climate simulation and trend-removed climate simulation.



895  
 896 Figure 8. Elasticity of total FPC with precipitation increased by 10% (a), air  
 897 air temperature increased by 1 °C (b), soil temperature increased by 1 °C (c), soil  
 898 moisture increased by 10% (d), CO<sub>2</sub> increased by 10% (e), and dominant elasticity  
 899 related with changes in precipitation, air temperature, soil temperature, soil  
 900 moisture and CO<sub>2</sub> (e). In (e), + (plus) and ◇ (diamond) represent positive and  
 901 negative elasticity, respectively.  
 902

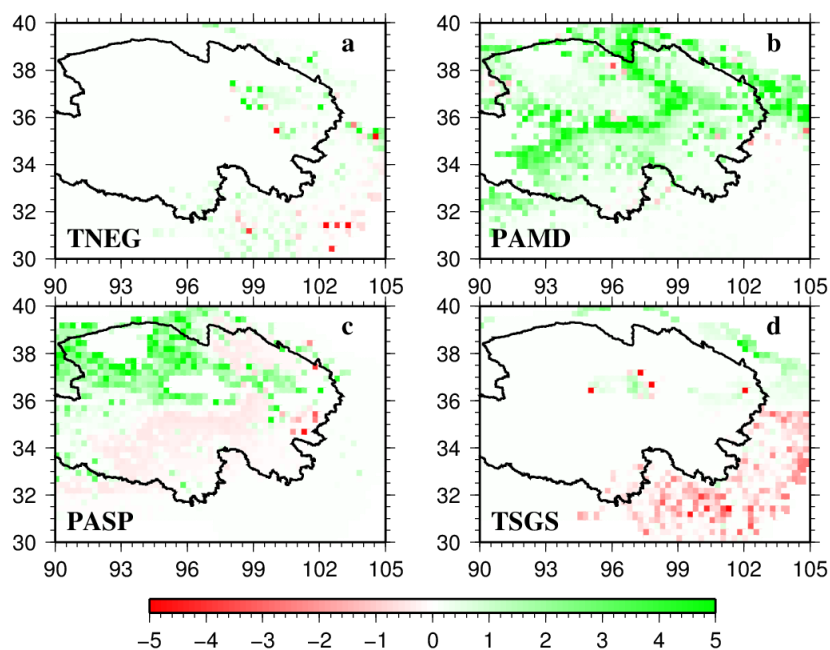


903  
904 Figure 9. Elasticity of individual FPCs with precipitation increased by 10% (a-d) and  
905 air temperature increased by 1 °C (e-h). TNEG: temperate needleleaf evergreen;  
906 PAMD: perennial alpine meadow; PASP: perennial alpine steppe; TSGS: temperate  
907 summer green scrub/grassland.  
908  
909  
910



911  
912  
913  
914

Figure 10. Elasticity of individual FPCs with +1 °C soil temperature increase (a-d) and 10% soil moisture increase (e-h).



915  
916  
917  
918

Figure 11. Elasticity of individual FPCs with 10% CO<sub>2</sub> increase.